Understanding atmospheric methane sub-seasonal variability over India

Yogesh K. Tiwari[1]*, Tania Guha[1], Vinu Valsala[1], Alfonso Saiz Lopez[2], Carlos Cuevas[2], Rafael P. Fernandez[2,3] and Anoop S. Mahajan[1]

[1]Indian Institute of Tropical Meteorology, Pune 411008, India

[2]Department of Atmospheric Chemistry and Climate, Institute of Physical Chemistry, Rocasolano, CSIC, Madrid, Spain.

[3]National Research Council (CONICET), FCEN-UNCuyo, UTN-FRM, Mendoza 5501, Argentina.

*Corresponding author: yktiwari@tropmet.res.in

Abstract

Atmospheric methane (CH_4) is considered to be one of the most important greenhouse gases due to its increasing atmospheric concentrations and the fact that it has a warming potential 28 times that of atmospheric carbon dioxide (CO_2). Over the Indian sub-continent, fluxes and transport both contribute towards CH_4 seasonal variability. Its intra-seasonal variability however is more complex as it is additionally influenced by monsoonal activity during the Asian Summer Monsoon (ASM) period. In this study, the intra-seasonal variability of atmospheric CH_4 is examined using ground-based observations at two sites located in the Southern Indian Peninsula, Sinhagad (SNG) and Cape Rama (CRI); and outputs from three different model simulations. Both, the ground based observations and multi-model simulations show that the dominant spectral variability of CH_4 is coherent with 20-90 day oscillations in the dynamics of the monsoon (termed hereafter as Intra-Seasonal Oscillations, ISOs). The multi-model analysis revealed that CH_4 is heavily influenced by advection due to this intra-seasonal variability. The simulations also display a clear northward propagation of CH_4 anomalies over India. The co-evolution of CH_4, outgoing long wave radiation (to represent convection) and OH radicals (proxy to CH_4 sinks) is presented. The study quantifies CH_4 variability at intra-seasonal timescales and also its spatial extent. The results suggest that the effect of ISOs on CH_4 needs to be considered along with the corresponding observations for future inverse modeling.

Key Words

Atmospheric CH_4 observations; model simulations; sub-seasonal variability; Indian sub-continent

1. Introduction

Emissions of atmospheric methane (CH_4) are of primary concern in India as it is one of largest emitters in the world (UNFCCC 2018 database; Ganesan et al., 2017). Quantifying these regional emissions is critical to understand the total effect of CH_4 on the global radiative forcing, which is estimated to be ~0.48±0.05 W m^{-2} by the end of the 20th century (Fifth Assessment Report, IPCC, 2013). Atmospheric CH_4 has both natural and anthropogenic origins. Wetlands act as the primary natural source (Cao et al., 1998), while rice paddies (Purkait et al., 2005; Khalil et al., 2008), livestock (Crutzen et al., 1986; Naqvi and Seijan, 2011), landfills (Chakraborty et al., 2011), combustion of fossil fuels, agricultural waste, bio-fuels (Howarth et al., 2011; Lelieveldet al., 1998) are the dominant anthropogenic sources. The main sink of atmospheric CH_4 is its reaction with hydroxyl radicals (OH) in the troposphere (Kirschke et al., 2013; Patra et al., 2014; Ghosh et al., 2015). Although the main sources and sinks of CH_4 are well known, estimating its budget has large uncertainties, especially at regional scales (Patra et al., 2016). Apparently, this difficulty is due to multiple and interconnected sources and sinks as well as transportation from the source areas to the measurement sites, which can vary greatly with seasons. This issue is further complicated by the shortage of observations that can capture these complex variations at a regional scale (Patra et al., 2016).

Tania et al., (2017) and Patra et al., (2016) have discussed in detail the seasonal variability of CH_4 over India. Here, CH_4 concentrations show large variations due to the dramatic seasonal reversals in upper and lower atmospheric circulation during the Asian Summer Monsoon (ASM) season. CH_4 seasonal variability over India is close to 200 ppb, showing a minimum during the ASM season (approx. 1800±20 ppb) and a maximum during the winter season (approx. 2000±30 ppb; Tania et al., 2017). In addition to the seasonal CH4 variability

68 during the Indian summer monsoon, it is expected that sub-seasonal variability and associated
69 atmospheric dynamics would affect the CH4 variability over India (Ravi Kumar et al., 2016;
70 Wang et al., 2006, Valsala et al., 2013). . Understanding the drivers behind these variability is
71 important considering that observations of CH_4 are used to identify sources and sinks by inverse
72 modeling (Ganesan et al., 2017).

73 Indian summer monsoon is broadly termed as a lower level atmospheric inflow of
74 oceanic air due to the land-ocean contrast established over the Asian-Indian Ocean region during
75 the summer season (June to September). Modulating this mean flow are the intermittent
76 perturbations of northward propagating convection, originating over the oceanic convergence
77 zone near the equatorial Indian Ocean and propagating northward towards the monsoon trough
78 over the land (i.e. Himalayan foothills). When these convections are active, the landmass
79 receives increased rainfall followed by a short spell of break days where the convection and
80 rainfall is weak (Sikka and Gadgil, 1980, Yasunari, 1979, Wang, 2006). This oscillation between
81 active and break spells of rain over India is termed as Intra-Seasonal Oscillations (ISOs) and is
82 best captured in the filtered (30-60 day band pass) outgoing longwave radiation (OLR)
83 anomalies. This sub-seasonal variability is hereon referred to as any variability within a band of
84 20-90 days. ISOs over the Indian region are prominent during the ASM season (June to
85 September) due to the northward migration of monsoonal convergent zones from the equatorial
86 regions to the foothills of Himalaya (Sikka and Gadgil, 1980;Yasunari, 1979). Considering the
87 fact that the seasonal cycle of CH_4 over India is predominantly determined by background
88 atmospheric dynamics rather than fluxes (Tania et al., 2017, Patra et al., 2016), the CH_4 ISOs are
89 also expected to follow similar dynamic footprints. However, a detailed study on this has not

been done hitherto and in this study we explore the ISOs from a dynamical perspective and their impact on the CH_4 observations.

High temporal resolution observations of CH_4 over India are still lacking, although, Cape Rama (Tiwari et al. 2011) and Sinhagad (Tiwari et al., 2014) are two examples where direct observations of greenhouse gases have been made over several years. Ravi Kumar et al. (2016) looked at the CO_2 ISOs at these two stations and found that the local biosphere fluxes, in response to monsoon ISOs, determine the CO_2 variability (Valsala et al., 2013). Preliminary analysis of CH_4 using the same methodology indicates that dominant peaks of variability between 20-90 days are seen in atmospheric CH_4. . Therefore, variability in CH_4 concentrations at ISO timescales deserves special attention.

In order to understand the CH_4 ISOs over India, we use model simulations in addition to surface observations in this study. The major foci of this study are to answer (i) what the patterns of atmospheric CH4 ISOs over India are; (ii) what the associations of CH4 variability at ISO time scales with the underlying atmospheric dynamics are; and (iii) what the major causes of CH4 ISOs over India are. . Answering the above questions is important considering that at present the observed CH_4 concentrations over India are used for interpreting the sources/sinks by statistical methods. Considering the negligible role of fluxes in controlling the atmospheric CH_4 seasonality over India (Guha et al., 2017), one may anticipate a similar relationship between CH_4 ISOs and fluxes. Hence, it is nontrivial to verify whether the state of the art atmospheric transport models capture such variability.

2. Data and Methodology

In this study we have used CH_4 observations from two ground-based stations i.e. Sinhagad (SNG) and Cape Rama (CRI); and CH_4 concentration fields simulated by three different models i) Laboratoire de Météorologie Dynamique (LMDz) model, ii) JAMSTEC's atmospheric chemistry transport model (ACTM), and iii) the 3D global chemistry Climate Model CAM-Chem. We have also used the Kalpana retrieved OLR dataset to identify the dynamical ISOs. Details of the models and OLR dataset are given in Sections 2.2 and 2.3.

2.1 Surface observations

A facility for measuring ambient mixing ratios of long-lived greenhouse gases (e.g. CO_2, CH_4 etc.), was established in India in 2009. This laboratory is equipped with Gas Chromatograph (GC) instrument, automatic air sampler, glass flasks, and flask evacuating-heating equipment. In this study, we used surface observations from two sites,

1) Sinhagad (SNG) is a mountain site located at the western boundary of India (200 km east of the Arabian Sea: 18.35° N, 73.75° E, 1600 m above mean sea level). Air Sampling location is free from any major vegetation in the vicinity. The prevailing wind speed during the time of sampling (i.e. noon) is comparatively low (0.5 – 1 m s^{-1}). Air samples at SNG are collected from top of 10 m tower at a weekly interval. Collected paired flask samples are analyzed at GC lab located at the Indian Institute of Tropical Meteorology (IITM) Pune. The analysis is calibrated using international standards provided by the WMO Central Calibration Laboratory (CCL) located at the National Oceanic and Atmospheric Administration (NOAA)/Earth System Research Laboratory (ESRL)/Global Monitoring Division (GMD), Boulder, Colorado, USA. The repeatability of the instrument was checked at regular interval using NOAA CH4 calibration

134 standards. To understand the reproducibility in measurement paired flask samples were analyzed
135 in the GC. The reproducibility was found to ±5 ppb (Tania et al., 2017). The entire monitoring
136 procedure air sample collection to GC analysis, were carefully examined. We made sure that the
137 collected samples are representative of large volume of atmosphere. Samples contaminated by
138 local sources are flagged and excluded from data analysis. Details of sample analysis, data
139 acquisition, and calibration procedures are described in Tiwari, et al., 2011; Ravi et al., 2014;
140 Tania et al, 2017. We adopted data analysis and quality control (QA/QC, outlier detection in raw
141 data, etc.) methods described in Dlugokencky et al., 1992. CH4 concentrations observed at SNG
142 during 2010-2013 are used in this study.

143 2) Cape Rama (CRI) is a coastal site in the state of Goa (15.08° N, 73.83° E, elevation =
144 50 m above mean sea level). CRI was maintained by the Commonwealth Scientific and
145 Industrial Research Organization (CSIRO) Atmospheric Research GASLAB (Global
146 Atmospheric Sampling Laboratory), air sampling was conducted from February 1993 until
147 January 2013, with a sampling gap between October 2002 and July 2009 (Francey et al., 1993;
148 Bhattacharya et al., 2009; Tiwari et al., 2011). The observations between July 2009 and January
149 2013 from CRI were considered for this study. Both the observational sites (SNG and CRI)
150 receive oceanic air masses during Indian summer monsoon season (JJAS) and continental air
151 masses during winter season (DJF) (Tiwari et al., 2014).

152 **2.2 Model Simulations**

153 We used three different models in this study:

154 **a) Laboratoire de Météorologie Dynamique zoom (LMDz)** is a general circulation model
155 simulated in a 'zoomed' version at horizontal resolution of 0.51° x 0.66° latitude by longitude,

39 sigma-pressure layers in the vertical, centered over the Indian sub-continent and adjoining areas (50°–130°E and 0–55°N). The model uses the advection scheme of Hourdin and Armengaud (1999) and deep convection is parameterized using Tiedtke (1989). The model considers the OH radical reaction as the main sink of atmospheric CH_4, which and the OH field is prescribed from a model simulation with a horizontal resolution of 3.75º x 1.9º involving the INCA (INteractions between Chemistry and Aerosols) tropospheric photochemistry scheme (Folberth et al., 2006; Hauglustaine et al., 2004). LMDz simulates CH_4 concentration fields by using surface fluxes and meteorology as an input. Surface fluxes used in the model are, i) anthropogenic emissions obtained from the Emission Database for Global Atmospheric Research (EDGAR) v4.2 FT2010 (http://edgar.jrc.ec.europa.eu) used at interannual time-scale and at 0.1° × 0.1° spatial resolution, ii) seasonal and 1° spatial resolution of rice cultivation emissions dataset obtained from Matthews et al., (1991), iii) wetland emissions climatology from Kaplan et al., (2006), iv) biomass burning emissions on interannual and seasonal timescales obtained from Global Fire Emissions Database (GFED) v4.1 (Randerson et al., 2012; Van Der Werf et al., 2017; http://www.globalfiredata.org/), v) climatological termite emissions obtained from Sanderson, (1996), vi) climatological ocean emissions obtained from Lambert and Schmidt, (1993), and vii) climatological soil uptake obtained from Ridgwell et al., (1999). The model uses meteorology obtained from the European Center for Medium Range Weather Forecast (ECMWF) reanalysis (ERA-I) dataset at a 6-hour interval (Bousquet et al., 2005). CH_4 concentrations were simulated during 2000-2015 and the first six years were considered as a spin-up time. These model simulations have been validated using observations at various locations over globe (Tania et al, 2017; Lin et al., 2018). Further details of the model and associated surface fluxes are given in Lin et. al, (2018).

b) The Atmospheric Chemistry Transport Model (ACTM) is developed by the Center for Climate System Research/National Institute for Environmental Studies/Frontier Research Center for Global Change (CCSR/NIES/FRCGC) atmospheric general circulation model (AGCM) based CTM (i.e JAMSTEC's ACTM ; Patra et al.,2009). It is a part of the transport model inter-comparison experiment TransCom-CH_4 (Patra et al., 2011a) and has been used in inverse modeling of CH_4 emissions from in situ observations (Patra et al., 2016). ACTM used here is with a horizontal resolution of $2.8^o \times 2.8^o$ with 67 sigma-pressure vertical levels. ACTM uses meteorology (produced online by AGCM) which is nudged with horizontal winds (U and V) and temperature from reanalysis fields from the Japan Meteorological Agency, version JRA-25 (Onogi et al., 2007). CH_4 concentrations were simulated during 2005-2014. First year was used as the model spin-up period and other nine years (2006-2014) were used for analysis in this study. Surfaces fluxes used in this model are, i) anthropogenic emissions from EDGAR v4.2 F2010, ii) wetland and biomass burning emissions from Fung et al., (1991), iii) emissions from rice paddies were obtained from Yan et al., (2009). The model uses monthly-mean OH concentrations fields obtained from full chemistry simulations for the troposphere (Sudo et al., 2002) and the stratosphere (Takigawa et al., 1999). Further details of the model and surface fluxes are available in Patra et al. (2009, 2011a, 2016) and Chandra et al. (2017).

c) NCAR Community Earth System Model with Chemistry (CAM-Chem) (version 4) (Lamarque et al., 2012) included in the CESM framework, was used in this study to estimate the CH_4 and OH tropospheric mixing ratios, as well as their temporal and spatial evolution. The simulation employed in this work is based on the Chemistry Climate Model Initiative – Reference Experiment (CCMI-REFC1) setup (Hegglin et al., 2014; Tilmes et al., 2016), and includes an updated halogen chemistry scheme (chlorine, bromine and iodine; Saiz Lopez et al.,

2012, 2014, 2016). Lower boundary conditions (LBC) for long-lived gases as well as the anthropogenic gas-phase emissions are equivalent to Fernandezet al., (2017). This model uses a horizontal resolution of 1.9ºx 2.5º and 56 sigma-pressure levels in the vertical. . The model was run in Specified Dynamic (SD) mode (Lamarque et al., 2012) using real meteorological fields from the Modern-Era Retrospective analysis for Research and Applications (MERRA) reanalysis database (Rienecker et al., 2011). OH concentrations are simulated in real time during the model run. Although data from 2006 to 2014 were employed in this work, the model run started from 2005 to reach steady state conditions.

To perform a thorough comparison between the observations and model simulations, the simulations are sampled at the same location and same time as the SNG and CRI observations. The main differences between the LMDz, ACTM, and CAM-Chem are: first, the special resolution, with ACTM and CAM-Chem having coarser resolution than LMDZ; second, all three models use different surface fluxes as inputs. Third, the meteorological fields used to solve model transport equation differ in the models. Thus, using such diverse models provides a thorough test of model-observation comparisons.

2.3 Satellite retrieved outgoing long-wave radiation (OLR)

The OLR data used in this study are from the Indian satellite Kalpana-1 (formerly METSAT-1) from 2006 to 2014. Kalpana-1 consists of a very high resolution radiometer (VHRR) used for meteorological applications. OLR values are an indicator of deep convection and are used for precipitation estimation (Xie et al., 1998). OLR data were estimated at a three hourly basis with a spatial resolution of 0.25º × 0.25º from the observed radiances of Kalpana-1 VHRR. More details

about the OLR data estimation from Kalpana-1 satellite are available in previous publications (Mahakur et al., 2013; Prakash et al., 2015).

2.4 Data analysis

In order to identify the dominant periodicities at sub-seasonal timescales, power spectrum analysis was done on the de-trended and de-seasonalized observed data from the two stations (SNG, CRI) and the three model simulations at the two selected stations. From this we have noted the dominant power spectra peaks at sub-seasonal time-scales. For further analysis of model CH4 concentrations at these sub-seasonal timescales, we have done the following. First, the annual (360 days) and semi-annual (180 days) cycles were removed from each year by employing harmonic filtering and the processed data were sampled for 121 days from 1st June to 30th September (JJAS). The JJAS days of each year were then stitched together into a single series (i.e. from 2006 to 2014 comprising a total of 1089 data points in time) and only the 20-90 day cycles were extracted by using harmonic filtering. Further details of the data analysis can be found in our past publications (Ravi et al., 2016).

In order to show the 20-90 day modes in the summer monsoon convection and associated dynamics, lead-lag spatial maps of OLR anomalies were produced (40 ^{o}E - 120 ^{o}E, 10 ^{o}S - 40 ^{o}N). This was obtained by regressing a central India averaged OLR index (from 20-90 day filtered OLR data as above) onto OLR anomalies for all the grid-points in the above domain with a lead or lag applied to OLR index within a range of -20 to +20 days. This processed data is used to understand the propagation of CH_4 anomalies at ISO scales during both active and break phases of the ASM. This analysis is defined as the 'lead-lag propagation'. The first day of the active spell is considered as 0^{th} day and the lead-lag analysis is done -20 to +20 days from this

benchmark. The dates for active rain spells for the years were identified from the OLR anomalies averaged over the Indian region using the method as in Pillai and Sahai (2016). A composite mean of all such events was used to delineate a -20 to +20 day evolution of OLR, CH_4 and OH anomalies and their coherent structures. Similar composite evolutions of break spells were also calculated.

Correlations between OLR and the processed CH_4 data for all 1089 time steps are calculated over the same domain (40^oE-120^oE, 10^oS-40^oN) at lead or lag for a range of days from -15 to 15. This has resulted in a total of 31 spatial correlation maps (and for each vertical level in the model). In order to identify the dominant correlation patterns between CH_4 and OLR, an empirical orthogonal functions (EOF) analysis over these 31 correlation maps was conducted (but only for LMDZ model as a test case). This helped to conclude on the meaningful dominant correlation patterns between CH_4 variability (at each grid point) and OLR (proxy for convection) at ISO timescales and provided information on how they oscillate with a specific lead or lag between them.

3. Results and Discussions

Figure 1 shows the measured surface CH_4 at the two observational sites, Sinhagad (SNG) and Cape Rama (CRI) along with the with model simulation outputs from the three models mentioned above. The correlation coefficient Pearson's r indicates that model simulations are in close agreement with the observations (Figure 1). CH_4 concentrations start increasing from September and peak in January, followed by a decreasing trend from February, reaching a minimum in August. An increasing trend is observed from 2009 to 2013. The trend and seasonal

cycle show similar patterns in the three models as well. A strong seasonal variation, with a peak-to-peak amplitude of about 300 ppb at SNG and 200 ppb at CRI is observed. SNG is located in the mountains (1600 m above mean sea level) whereas CRI is located closer to the coast with low vegetation in the vicinity. Lin et al., 2018 evaluated the LMDz model performance using various surface observations, including Indian sites SNG, CRI, Hanle, Pondicherry, and Port Blair, over South and South East Asia. Results show that the model simulations agree with the observations on an annual and seasonal scale. Further, Bhattacharya et al., (2009) and Tiwari et al., (2011) evaluated the ACTM model capabilities over India using surface observations at CRI, again showing a good match between observations and model simulations.

The power spectrum presented in Figure 2, indicates that there are clear spectral peaks at 27, 89 and 116 days for observations at SNG. For CRI, the spectral peaks at 70 and 114 days are clearly visible. The corresponding model outputs at SNG show spectral peaks at 91, 122 and 183 days (for LMDZ); 19, 23 and 122 (for ACTM); 32, 91 and 122 (for CAM-Chem). The model outputs at CRI show spectral peaks at 28, 39 and 112 days (for LMDZ); 27, 31 and 112 (for ACTM); 28, 37 and 112 (for CAM-Chem). These analyses indicate that atmospheric CH_4 is embedded with an ISO signal with a predominating 20-90 day cycle. Similar ISO structures in atmospheric CO_2 were identified earlier (Ravi Kumar et al., 2016). However, one of the reasons for that was the corresponding variability in fluxes rather than in atmospheric dynamics (Valsala et al., 2013). In case of CH_4, the ISOs are expected to be dominated by atmospheric dynamics rather than fluxes because flux variability is not a determining factor in the seasonal cycle of atmospheric CH_4 over India (Tania et al., 2017). Moreover, all the models here are run with climatological monthly mean CH_4 fluxes and therefore the inherent ISO variability in model CH_4

289 concentrations cannot origin from the fluxes but would be driven more by dynamics or from
290 atmospheric chemistry.

291 Figure 3 depicts the lead-lag regressions for OLR anomalies based on an index of OLR
292 averaged over the Indian region (Figure 3). Here, the negative OLR anomalies stand for
293 convection and organized rain. As time progresses from -20 to +20 days, convection from the
294 equatorial oceanic region appears to move northward and the cycle terminates by +20 days over
295 land. The corresponding CH_4 anomaly propagations are represented as latitude-time plots of
296 composite CH_4 evolutions for active and break rainy spells (see Section 2.4 for details) for three
297 different vertical levels (Figure 4). The area averaged for these plots is over a region between 55^o
298 E and 110^o E and shown for the surface (1000 mb), middle troposphere (650 mb) and upper
299 troposphere (230 mb) for each of the three models considered here.

300 A conspicuous feature revealed in the composite analysis is a clear northward
301 propagation of CH_4 anomalies with an amplitude of ±10 ppb and at a speed of approximately 1.5^o
302 latitude per day. On the day that the active spell commences (i.e. at zero on the time axis), the
303 CH_4 concentration anomalies switch from positive to negative at the surface, middle and upper
304 troposphere. This is visible in the three model outputs analyzed here, although with some
305 differences from model to model. During the active spells over the land, the convection is at its
306 peak and CH_4 appears to reduce in concentration at the surface and is also slightly lower in the
307 middle troposphere but hardly any change is seen in the upper troposphere. This phenomenon
308 continues from 0 to +15 days. This indicates that due to convection, oceanic air masses that have
309 less CH_4 get transported from the lower troposphere to the middle troposphere over India. At the
310 upper troposphere (230 mb) the CH_4 anomalies during and following the active phase are rather
311 weak.

An opposite trend in CH_4 anomalies is visible during the break phase as expected (Figure 4). On the day that the break spell commences and during its progression from 0 to +10 days, the CH_4 concentration anomalies at the surface switch from negative to positive. This is also visible in the middle troposphere and more distinctly in the upper troposphere. The background mean CH_4 concentrations over India during summer have been previously reported by Tania et al., (2017). According to their study, during the summer monsoon season over India, surface CH_4 is lower than in the upper troposphere, which indicates a dilution effect of CH_4 due to the advection of oceanic air-masses from the near-equatorial region towards the Indian continent (see also Patra et al., 2016). Convection during the active period transports these air masses with low CH_4 aloft. However, during the break period large scale subsidence over India brings the upper tropospheric air-mass downwards. These air masses are enriched in CH_4 as compared to the surface air. This explains the strong CH_4 anomalies in the upper and middle troposphere during break period compared to the surface. Therefore, the active and break composite responses of CH_4 appear as a see-saw pattern vertically (compare Figure 4, panel 'a' and 'f' in all three models).

The atmospheric CH_4 budget is controlled by the surface fluxes, transport and sinks, mainly due to hydroxyl radicals (OH). Therefore the role of OH in modulating the intra-seasonal signal of CH_4 has to be quantified and we calculate the active-break composite of CAM-Chem simulated OH (Figure 5) using the same method as used for CH_4. It is observed that OH does not show an ISO variability similar to that of CH_4. Thus, it appears that OH does not have any discernible impact on the CH_4 variability at ISO timescales. This is an expected result since a change of ±10 ppb in CH_4 would not be expected to have a large impact on the oxidizing capacity of the troposphere on such short timescales. Further, we estimated the loss of CH_4

through reactions with OH ($k = 1.85 \times 10^{-12} e^{(-1690/T)}$; Atkinson et al., 2004) during the ASM season (JJAS). The CH_4 lifetime is approximately 782 days assuming the mean OH concentrations above the Indian sub-continent during the ASM (0.06 pptv). To cause a reduction of about 10 ppb, it would take about 4 days. This result indicates that the change in CH_4 during the active and break spells is within the oxidation timescale and hence OH oxidation could play a role in addition of transport of different air masses. However, the lack of a large difference in the OH concentrations between the active and break spells indicates that the difference in CH_4 between the two spells is most probably driven by transport rather than oxidation chemistry, as can be seen through the OH and CH_4 ISOs.

In order to understand the spatio-temporal locking of CH_4 variability in relation with convection, a correlation between OLR and CH_4 anomalies at each grid point over the analyzed domain was conducted (see Section 2.4). OLR lead-lag analysis spanning -15 to +15 days with respect to the CH_4 data was conducted and the correlations for each lead-lag was analyzed. A side-by-side analysis of all lead-lag at all levels of spatiotemporal correlations appears as chaotic in space and time, because of which we employ EOF analysis on correlation maps (see Section 2.4). CH_4 variability in the 20-90 day mode in the model simulations (also in the observations) is connected to the convection and its northward movement as per the dynamics of the ASM. At each lead and lag from -15 to +15 days, the CH_4 and OLR are correlated in space and thus there are 31 maps of correlations for each level above the surface. To summarize how the correlation itself changes from a lead-lag of -15 to +15 days, EOF analysis of correlations is presented. Figure 6 thus enables us to conclude the joint spatio-temporal variability of the 20-90 day mode in CH_4 oscillations in connection with the Asian monsoon. Figure 6 shows the dominant mode EOFs of correlation coefficients (EOF-1 and EOF-2) in space and their principle component in

time composed of -15 to +15 days of lead-lag axis. Here the -15 means that the OLR lags CH_4 by 15 days and +15 means that the OLR leads CH_4 by 15 days. At the surface level (1000 mb), the EOF-1 pattern of correlations is positive over India with negative limps over the Bay of Bengal and north-western region of India (Figure 6, Panel 'a'). The patterns are largely organized in space indicating that a large-scale feature exists between CH_4 and convection. The pattern of surface level (1000 mb) PC-1 peaks at a lag of -6 days (i.e. OLR lagged CH_4 by 6 days). However, the reason for such a lag is not clear from the present analysis. It changes sign at a lead of +9 days (Figure 6, lower left panel). Overall the cycle completes in ~50 days as the quasi-sine wave shape seen in principle components (PC). EOF-2 (Figure 6, Panel 'd') has an entirely different structure, with negative correlations accumulated over the Indian land mass extending all the way to the northern part of the domain, with a positive patch over the north Arabian Sea. The PC-2 (Figure 6, lower left panel) suggests that the pattern peaks in this shape at almost zero-lag between CH_4 and OLR. The cycle of this mode also completes a quasi-cosine wave shape in about 50 days. The correlation between PC-1 and PC-2 is almost zero indicating that the modes are orthogonal. Both modes are of significant variances.

There is no clear harmony revealed between EOFs at the surface (1000 mb) and the middle troposphere (650 mb) (Figure 6, Panel 'a', 'b', 'd' and 'e'). In the middle troposphere (650 mb), and for EOF-1, the correlations are negative between CH_4 and OLR all over India, while the surface has positive correlation over most of India aside from a negative correlation over the northwestern region. The PC-1 of surface (1000 mb) and middle troposphere (650 mb) is quasi-coherent, albeit with slight inter-lag of two days (PC-1 of Figure 6 'lower left' and 'mid' Panel). The EOF-2 appears to be anti-correlated between surface (1000 mb) and middle troposphere (650 mb).

In the upper atmosphere (230 mb), the EOF-1 correlations are wide-spread through an east-west direction over the land. The corresponding PC-1 (Figure 6, 'lower right' panel) indicates that this is an in-situ correlation between CH_4 and OLR because the pattern peaks when the lead-lag is zero. A possibility could be that in the presence of moisture in the lower atmosphere, the CH_4-OLR coupling has a lag of 6 days, which is close to zero in more dry conditions such as the upper atmosphere (230 mb). Whether the role of absorption bands of CH_4 and water vapor are interlinked or not is unclear from this study. EOF-2 in the upper troposphere (230 mb) shows more chaotic features (Figure 6f).

4. Summary and Conclusions

The main inferences derived from this study can be summarized in the following six points. (i) Atmospheric CH_4 has short term variability over India during the monsoon period. The power spectrum analyses of observations and models indicate that atmospheric CH_4 is broadly embedded with a 20-90 day ISO signal. (ii) Monsoon dynamics control the atmospheric CH_4 ISOs. (iii) Active to break and break-active transitions of monsoon ISOs as revealed in the OLR anomalies are equally imprinted on the atmospheric CH_4 variability over India, with negative (positive) CH_4 anomalies from the date of onset of active (break) to next 15 days. (iv) The strengths of CH_4 ISO anomalies are stronger (weaker) at surface (upper atmosphere) for active (break) periods. (v) There is as clear northward propagation of CH_4 anomalies at an amplitude of ±10 ppb and at a speed of approximately 1.5^o latitude per day. (vi) OH does not have a controlling impact on the CH_4 variability of amplitude ±10 ppb in the atmosphere at ISO timescales.

Acknowledgements

The Indian Institute of Tropical Meteorology is funded by the Ministry of Earth Sciences, India. We are thankful to Dr. Prabir Patra (JAMSTEC, Yokohama, Japan), and Michel Ramonet & Xin Lin (LSCE Paris France) for providing ACTM and LMDZ model simulations respectively for this study. Also, we are thankful to research team at IITM Pune India who estimated Kalpana-1 OLR data and made available for this study. SNG data is described in Tiwari et al., (2014) and is available upon request. CRI data is available at World Data Centre for Greenhouse Gases (WDCGG) (https://gaw.kishou.go.jp/). Kalpana OLR data is available at (https://tropmet.res.in/static_pages.php?page_id=144).

References

Atkinson, R., Baulch, D. L., Cox, R. A., Crowley, J. N., Hampson, R. F., Hynes, R. G.,Jenkin, M. E., Rossi, M. J., and Troe, J. (2004). Evaluated kinetic and photochemical data for atmospheric chemistry: Volume I-gas phase reactions of Ox, HOx, NOx and SOx species. *Atmos. Chem. Phys.*, 4, 1461-1738, 10.5194/acp-4-1461-2004, 2004

Bhattacharya, S.K., Borole, D. V., Francy, R. J., Allison, C. E., Steele, L. P., Krummel, P., Langenfelds, R., Masarie, K. A., Tiwari, Y. K., Patra, P. K. (2009). Trace gases and CO2 isotope records from Cabo de Rama, India. *Current Science*, 97(9), 1336–1344

Cao, M., Gregson, K., Marshall, S. (1998). Global methane emission from wetlands and its sensitivity to climate change. *Atmos. Environ.*, 32 (19), 3293e3299. http://dx.doi.org/10.1016/S1352-2310 (98) 00105-8

Chakraborty, M., Sharma, C., Pandey, J., Singh, N., Gupta, P.K. (2011). Methane emission estimation from landfills in Delhi: a comparative assessment of different methodologies. *Atmos. Environ*, 45 (39), 7135e7142. http://dx.doi.org/10.1016/jatmosenv.2011.09.015

Chandra, N., Hayashida, S., Saeki, T., and Patra, P. (2017). What controls the seasonal cycle of columnar methane observed by GOSAT over different regions in India?.*Atmos. Chem. Phys.*, 17, 12633–12643, 2017, https://doi.org/10.5194/acp-17-12633-2017

Crutzen, P.J.,Aselmann, I.and Seiler,W.(1986).Methane productionbydomesticanimals,wild ruminants,otherherbivorousfauna,andhumans. *Tellus*38B,271-284.

Dlugokencky, E. J., L. P. Steele, P. M. Lang and K. A. Masarie, (1994), The growth rate and distribution of atmospheric methane, Journal of Geophysical Research, 99, D8, 17, doi:10.1029/94JD01245

EDGAR (2014). European Commission, J. R. C. (JRC)/Netherlands E. A. A. (PBL). Emission Database for Global Atmospheric Research (EDGAR), release EDGARv4.2 FT2012, available at http://edgar.jrc.ec.europa.eu. (2014)

Fernandez, R. P., Kinnison, D. E., Lamarque, J. F., Tilmes, S., Saiz-Lopez, A.(2017). Impact of biogenic very short-lived bromine on the Antarctic ozone hole during the 21st century.*Atmos. Chem. Phys.*, *17*(3), 1673-1688

Folberth, G. A., Hauglustaine, D. A., Lathière, J., and Brocheton, F. (2006). Interactive chemistry in the Laboratoire de MétéorologieDynamique general circulation model: model description and impact analysis of biogenic hydrocarbons on tropospheric chemistry, *Atmos. Chem. Phys.*, 6, 2273–2319,https://doi.org/10.5194/acp-6-2273-2006, 200

Francey, R.J., Steele, L.P., Langenfelds, R.L., Lucarelli, M.P., Allison, C.E., Beardsmore, D.J., et al. (1993). Global Atmospheric Sampling Laboratory (GASLAB): supporting and extending the Cape Grim trace gas programs. Baseline Atmospheric Program (Australia).edited by R.J. Francey, A.L. Dick and N. Derek, pp 8 - 29*, Bureau of Meteorology and CSIRO Division of Atmospheric Research, Melbourne, Australia*

Ganesan, A. L., Rigby, M., Lunt, M. F., Parker, R. J., Boesch, H., Goulding, N., Umezawa, T., Zahn, A., Chatterjee, A., Prinn, R. G., Tiwari, Y. K., van der Schoot, M., and Krummel, P. B. (2017), Atmospheric observations show accurate reporting and little growth in India's methane

emissions. *Nature Communications*, 8:836, DOI:10.1038/s41467-017-00994-7 www.nature.com/naturecommunications

Ghosh, A., Patra, P. K., Ishijima, K., Umezawa, T., Ito, A., Etheridge, D. M., Sugawara, S., Kawamura, K., Miller, J. B., et al. (2015).Variations in global methane sources and sinks during 1910–2010.*Atmos. Chem. Phys.*, 2595-2612, doi:10.5194/acp-15-2595-2015

Guha T., Tiwari, Y. K., Valsala, V., Lin, X., Ramonet, M., Mahajan, A., Datye, A., Ravi Kumar, K. (2017). What controls the atmospheric methane seasonal variability over India?,*Atmospheric Environment*, 175, 83–91, https://doi.org/10.1016/j.atmosenv.2017.11.042

Hauglustaine, D. A., Hourdin, F., Jourdain, L., Filiberti, M.-A., Walters, S., Lamarque, J.-F., and Holland, E. A. (2004). Interactive chemistry in the Laboratoire de MétéorologieDynamique general circulation model: Description and background tropospheric chemistry evaluation, J. Geophys. Res., 109, D04314, doi:10.1029/2003JD003957

Hegglin, M. I., Lamarque, J.-F., Eyring, V., Hess, P., Young, P. J., Fiore, A. M., et al. (2014). IGAC/SPARC Chemistry-Climate Model Initiative (CCMI) 2014 Science Workshop, SPARC Newsl., 43(July), 32–35, 2014

Hourdin, F., Armengaud, A. (1999). Test of a hierarchy of finite-volume schemes for transport of trace species in an atmospheric general circulation model. *Mon. Weather Rev.*, 127, 822– 837

Howarth, R. W., Santoro, R., Ingraffea, A. (2011). Methane and the greenhouse-gas footprint of natural gas from shale formations.*Climate Change*, 106 (4), 679-690. DOI: 10.1007/s10584-011-0061-5

IPCC: Climate Change. (2013). The Physical Science Basis. Contribution of Working Group I to the Fifth Assessment Report of the Intergovernmental Panel on Climate Change, *Cambridge University Press, Cambridge*, 2013

Kaplan, J. O., Folberth, G., and Hauglustaine, D. A. (2006). Role of methane and biogenic volatile organic compound sources in late glacial and Holocene fluctuations of atmospheric methane concentrations. *Global Biogeochem. Cycles*, 20(2), GB2016, doi:10.1029/2005GB002590, 2006

Khalil, M. A. K., M. J. Shearer, R. A. Rasmussen, C. Duan, and L. Ren (2008), Production, oxidation, and emissions of methane from rice fields in China, *J. Geophys. Res.*, 113, G00A04, doi:10.1029/2007JG000461

Kirschke, S., Bousquet, P., Ciais, P., Saunois, M., Canadell, J. G., Dlugokencky, E. J., et al. (2013). Three decades of global methane sources and sinks. *Nature Geoscience*, 813-823, DOI: 10.1038/NGEO1955

Lamarque, J. F., et al. (2012), CAM-chem: description and evaluation of interactive atmospheric chemistry in the Community Earth System Model. *Geosci. Model Dev.*, *5*(2), 369-411

Lelieveld, J.,Cmtzen, P. J., and Dentener, F. J. (1998).Changingconcentration,lifetimeandclimateforcingofatmosphericmethane,*Tellus*,Ser.B,50, 128-150,1998

Rienecker, M. M., et al. (2011). MERRA: NASA's Modern-Era Retrospective Analysis for Research and Applications. *J. Clim.*, *24*(14), 3624-3648

Lambert, G. and Schmidt, S. (1993). Reevaluation of the oceanic flux of methane: Uncertainties and long term variations. *Chemosphere*, 26(1–4), 579–589, doi:http://dx.doi.org/10.1016/0045-6535(93)90443-9

Lin, X., Ciais, P., Bousquet, P., Ramonet, M., Yin, Y., et al. (2018). Simulating CH_4 and CO_2 over South and East Asia using the zoomed chemistry transport model LMDzINCA. *Atmos. Chem. Phys.*, 18, 9475-9497, 2018, https://doi.org/10.5194/acp-18-9475-2018

Mahakur, M. ,Prabhu, A., Sharma, A. K. , Rao, V. R., Senroy, S., Singh, R., Goswami, B.N. (2013). A high-resolution outgoing longwave radiation dataset from Kalpana-1 satellite during 2004–2012.*Current Science*, Vol. 105, No. 8, 25 Oct. 2013

Naqvi, S., M.K., Seijan, V. (2011). Global climate change: role of livestock. *Asian J.Agric. Sci.*, 31 (1), 19e25

Onogi, K., Tsutsui, J., Koide, H., Sakamoto, M., Kobayashi, S., Hatsushika, H., Matsumoto, T.,Yamazaki, N., Kamahori, H., Takahashi, K., Kadokura, S., Wada, K., Kato, K., Oyama, R., Ose, T.,Mannoji, N., and Taira, R. (2007).The JRA-25 reanalysis, *J. Meteorol.Soc. Jpn.*, 85, 369–432, 2007

Patra, P. K., Takigawa, M., Ishijima, K., Choi, B. C., Cunnold, D.,Dlugokencky, E. J., Fraser, P., Gomez-Pelaez, A. J., Goo, T. Y.,Kim, J. S., Krummel, P., Langenfelds, R., Meinhardt, F., Mukai, H., O'Doherty, S., Prinn, R. G., Simmonds, P., Steele, P.,Tohjima, Y., Tsuboi, K., Uhse, K., Weiss, R., Worthy, D., andNakazawa, T. (2009).Growth rate, seasonal, synoptic, diurnal variationsand budget of methane in lower atmosphere, *J. Meteorol. Soc.Jpn.*, 87, 635–663, https://doi.org/10.2151/jmsj.87.635, 2009.

516 Patra, P. K., Houweling, S., Krol, M., Bousquet, P., Belikov, D.,Bergmann, D., Bian, H.,
517 Cameron-Smith, P., Chipperfield, M. P.,Corbin, K., Fortems-Cheiney, A., Fraser, A., Gloor, E.,
518 Hess, P.,Ito, A., Kawa, S. R., Law, R. M., Loh, Z., Maksyutov, S., Meng,L., Palmer, P. I., Prinn,
519 R. G., Rigby, M., Saito, R., and Wilson,C. (2011a).TransCom model simulations of CH4

520 and related species:linking transport, surface flux and chemical loss with CH4 variability in the
521 troposphere and lower stratosphere, *Atmos. Chem.Phys*., 11, 12813–12837,
522 https://doi.org/10.5194/acp-11-12813-2011, 2011a

523 Patra, P. K.**,** Krol, M. C., Montzka, S. A., Arnold, T., Atlas, E. L., Lintner, B. R., Stephens, B.
524 B., et al. (2014).Observational evidence for interhemispheric hydroxyl parity.*Nature*, 513, 219-
525 223

526 Patra P., Saeki T., Dlugokencky, E. J.,Ishijima, K., Umezawa, T., Ito, A., Aoki, S., Morimoto, S.,
527 Kort, E. A.,Crotwell A. (2016). Regional Methane emission estimation based on observed
528 atmospheric concentrations (2002-2012). *Journal of Meteorological Society of Japan*, 94(1), 85-
529 107

530 Prakash, R., Singh, R.K.,Srivastava, H.N. (2015). Outgoing long wave radiation (OLR) from
531 Kalpana satellite prior to Nepal earthquake of April 25, 2015. *International Journal of Research*
532 *in Engineering and Technology,* Volume: 04 Issue: 07 | July-2015, eISSN: 2319-1163 | pISSN:
533 2321-7308, Available @ http://www.ijret.org

534 Purkait, N. N., Sengupta M. K., De, S., Chakraborty, D. K. (2005). Methane emission from the
535 rice fields of West Bengal over decades. *Indian J. Radio Spac Phys.*, 34, 255-263

536 Ravi Kumar, K.**,** Tiwari**,** Y. K.**,** **V**alsala, V., Murtugudde, R. (2014). On understanding of land-
537 ocean CO_2 contrast over Bay of Bengal: A case study during 2009 summer monsoon.
538 *Environmental Science and Pollution Research,* Volume 21, Issue 7, April 2014, Page 5066-
539 5075, DOI: 10.1007/s11356-013-2386-2

540 Ravi Kumar, K., Valsala, V., Tiwari, Y. K., Revadekar, J. V., Pillai, P.,Chakraborty,S.,
541 Murtugudde, R. (2016). Intra-seasonal variability of atmospheric CO2 concentrations over India
542 during summer monsoons.*Atmos. Environ.*, 142 (2016) 229e237, DOI:
543 10.1016/j.atmosenv.2016.07.023

544 Ridgwell, A. J., Marshall, S. J. and Gregson, K. (1999). Consumption of atmospheric methane by
545 soils: A process-based model. *Global Biogeochem. Cycles*, 13(1), 59–70,
546 doi:10.1029/1998GB900004, 1999

547 Saiz-Lopez, A., Lamarque, J.-F., Kinnison, D. E., Tilmes, S., Ordóñez, C., Orlando, J. J., Conley,
548 A. J., Plane, J. M. C., Mahajan, A. S., Sousa Santos, G., Atlas, E. L., Blake, D. R., Sander, S. P.,
549 Schauffler, S., Thompson, A. M., and Brasseur, G.: Estimating the climate significance of
550 halogen-driven ozone loss in the tropical marine troposphere, Atmos. Chem. Phys., 12, 3939–
551 3949, doi:10.5194/acp-12-3939-2012, 2012.

552 Saiz-Lopez, A., Fernandez, R. P., Ordóñez, C., Kinnison, D. E., Gómez Martín, J. C., Lamarque,
553 J.-F., and Tilmes, S.: Iodine chemistry in the troposphere and its effect on ozone, Atmos. Chem.
554 Phys., 14, 13119–13143, doi:10.5194/acp-14- 13119-2014, 2014.

555 Saiz-Lopez, A. and Fernandez, R. P.: On the formation of tropical rings of atomic halogens:
556 Causes and implications, Geophys. Res. Lett., 43, 2928–2935, 2016.

557 Sanderson, M. G. (1996). Biomass of termites and their emissions of methane and carbon
558 dioxide: A global database. *Global Biogeochem. Cycles*, 10(4), 543–557,
559 doi:10.1029/96GB01893, 1996

560 Sikka, D. R., and Gadgil, S.(1980).On the maximum cloud zone andthe ITCZ over Indian
561 longitudes during the southwest monsoon.Mon. Wea. Rev.,108,1840–1853

562 Sudo, K., Takahashi, M., Kurokawa, J., and Akimoto, H. (2002). CHASER: A global chemical
563 model of the troposphere 1. Model description.*J. Geophys. Res.*, 2002, 107, 4339

564 Takigawa, M., Takahashi, M., andAkiyoshi, H. (1999). Simulation of ozone and other chemical
565 species using a Center for Climate System Research/National Institute for Environmental Studies
566 atmospheric GCM with coupled stratospheric chemistry. *J. Geophys. Res.*, 104, 14003–14018

567 Tiwari, Y. K., Ravi Kumar, K. (2011). Glass flask air sample analysis through gas
568 chromatography in India: implications for constraining CO_2 surface fluxes. *WMO/GAW Report*
569 *No. 194*, WMO/TD-No.1553, April 2011.

570 Tiwari,Y. K.**,**Vellore, R. K., Ravi Kumar, K., Schoot, M. V. D., Cho, C. (2014). Influence of
571 monsoons on atmospheric CO_2 spatial variability and ground-based monitoring over India. *Sci.*
572 *of The Total Envi.*, 490 (15),570–578, http://dx.doi.org/10.1016/j.scitotenv.2014.05.045

573 Tiedtke, M. (1989).A comprehensive mass flux scheme for cumulus parameterization in large-
574 scale models.*Mon. Weather Rev*., 117, 1179–1800.

575 Tilmes, S., et al. (2016). Representation of the Community Earth System Model (CESM1)
576 CAM4-chem within the Chemistry-Climate Model Initiative (CCMI). *Geosci. Model Dev.*, 9(5),
577 1853-1890.

578 Valsala, V., Tiwari, Y. K., Pillai, P., Roxy, M., Maksyutov, S., Murtugudde, R. (2013).
579 Intraseasonal variability of terrestrial biospheric CO_2 fluxes over India during summer
580 monsoons. *JGR-Biogeosciences*, 28 May 2013, VOL. 118, pp 752–769, DOI:
581 10.1002/jgrg.20037; ISSN 2169-8961

582 Wang, B., Webster, P., Kikuchi, K., Yasunari, T., and Qi, Y. (2006).Boreal summer quasi-
583 monthly oscillation in the global tropics.*Climate Dyn.*, 27, 661-675

584 Xie, P., Arkin, P. A. (1998). Global monthly precipitation estimates from satellite-observed
585 outgoing longwave radiation. *J. Climate*, 1998, 11, 137–164

586 Yasunari, T. (1979). Cloudiness fluctuation associated with theNorthern Hemisphere summer
587 monsoon.*J. Meteor. Soc. Japan*,57,227–242
588

589 **Figures**

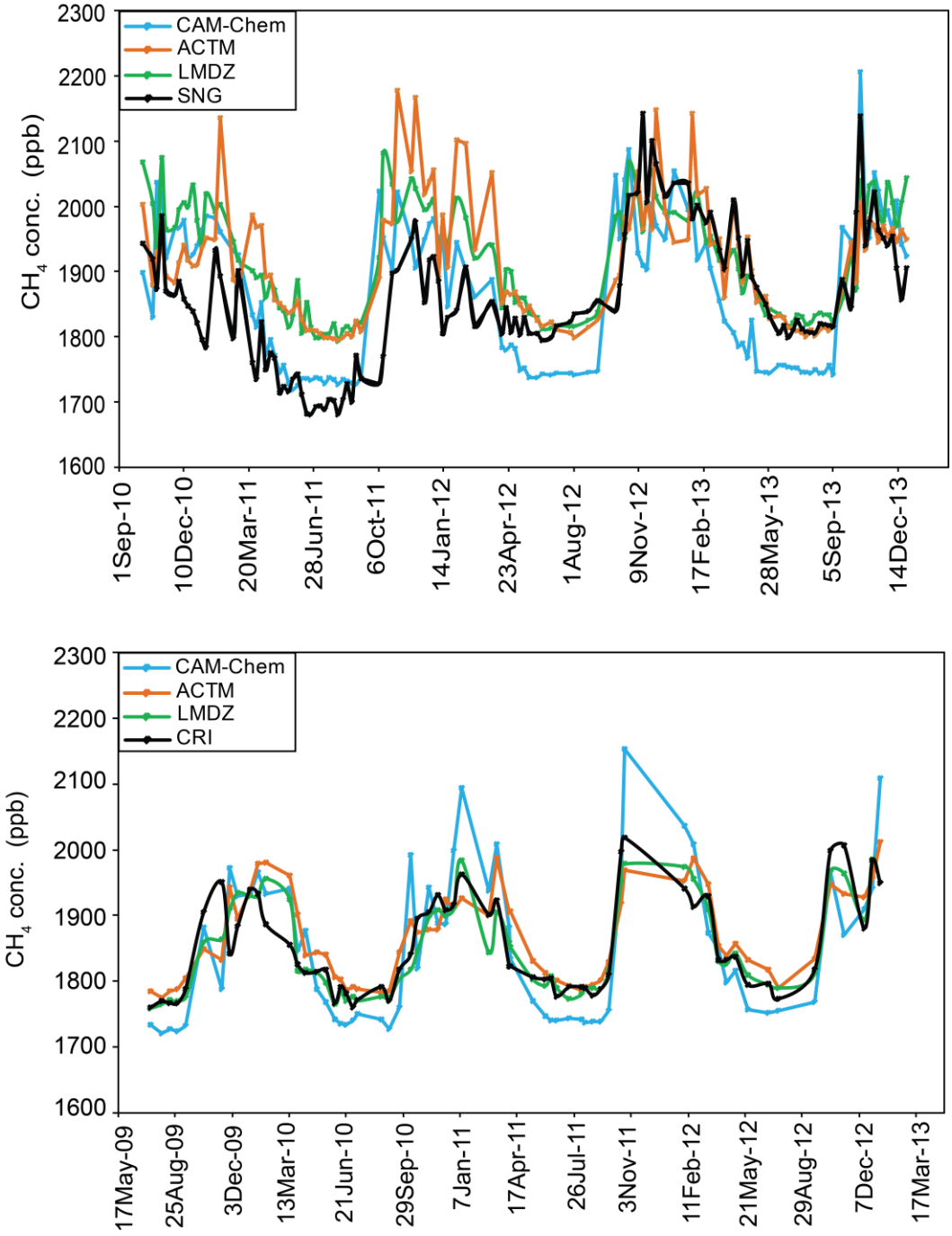

590

591 **Figure 1:** Atmospheric CH_4 concentration (ppb) observations at surface sites in India Sinhagad
592 (SNG) (top panel) and Cape Rama (CRI) (bottom panel) compared with model simulations
593 CAM-Chem, ACTM, and LMDZ. Correlation coefficient Pearson's r is as: SNG vs LMDZ =

+0.699; SNG vs ACTM = +0.642; SNG vs CAM-Chem = +0.681; CRI vs LMDZ = +0.926; CRI vs ACTM = +0.825; CRI vs CAM-Chem = +0.8260)

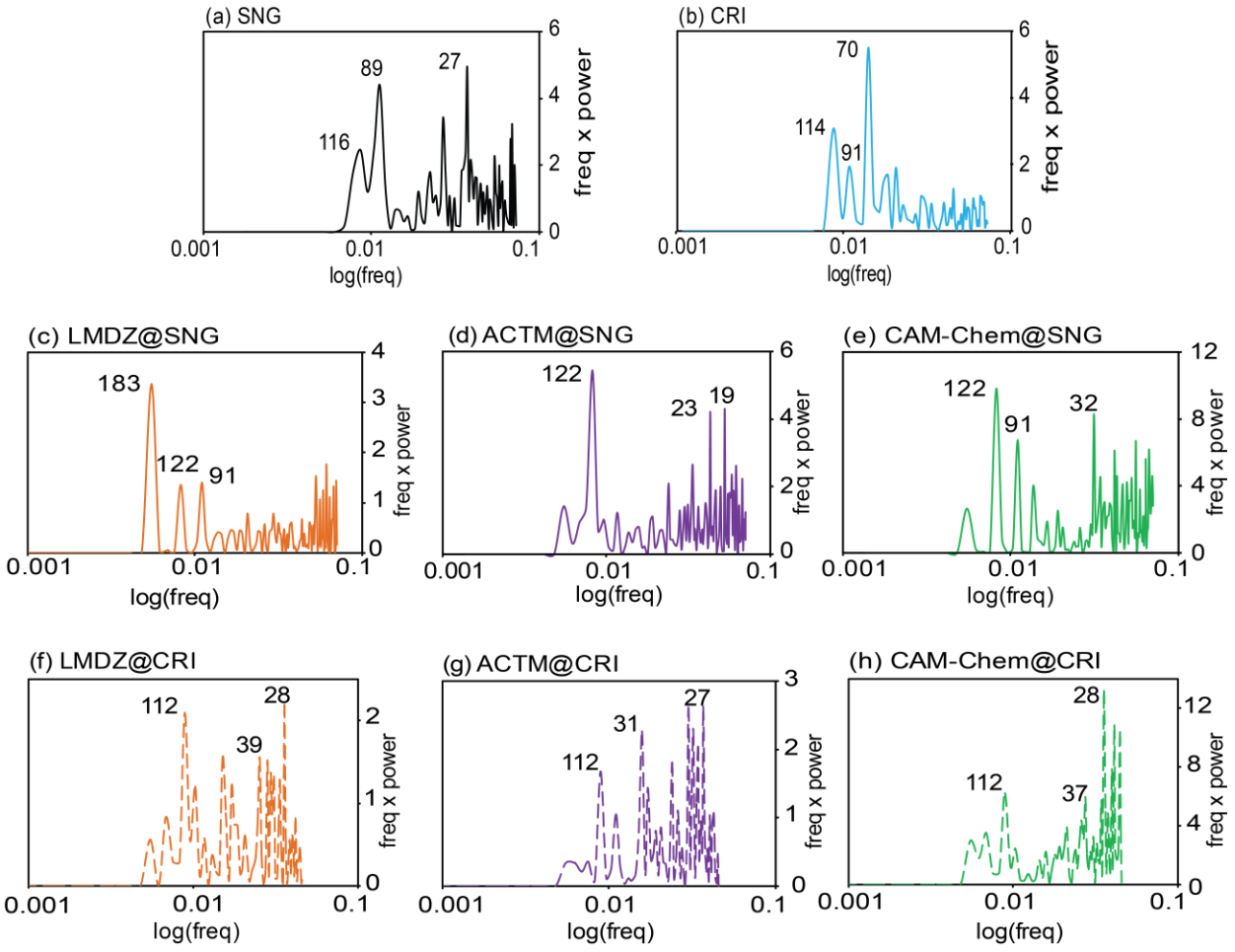

Figure 2: Power spectrum of de-trended and de-seasonalized observed surface atmospheric CH_4 mixing ratios at a) Sinhagad (SNG) b) Cape Rama (CRI), and correspondingly sampled model simulations c) LMDZ d) ACTM and e) CAM-Chem.

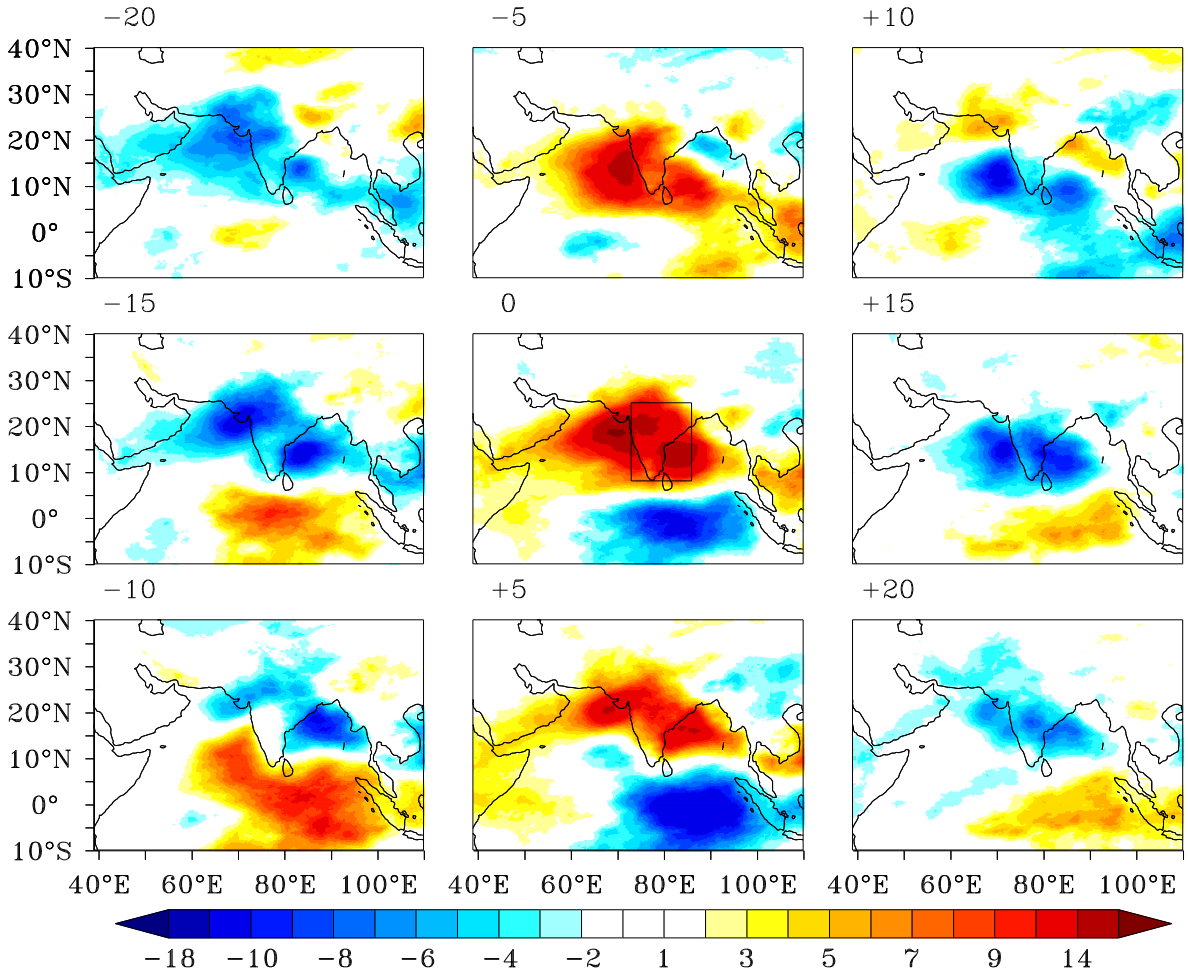

Figure 3: Lead-lag regression analysis of OLR anomalies (Wm^{-2}) onto a normalized index of OLR averaged over the box shown in the figure. The regressions analysis was done using JJAS daily anomalies data for 2006-2015, assembled over 9 years.

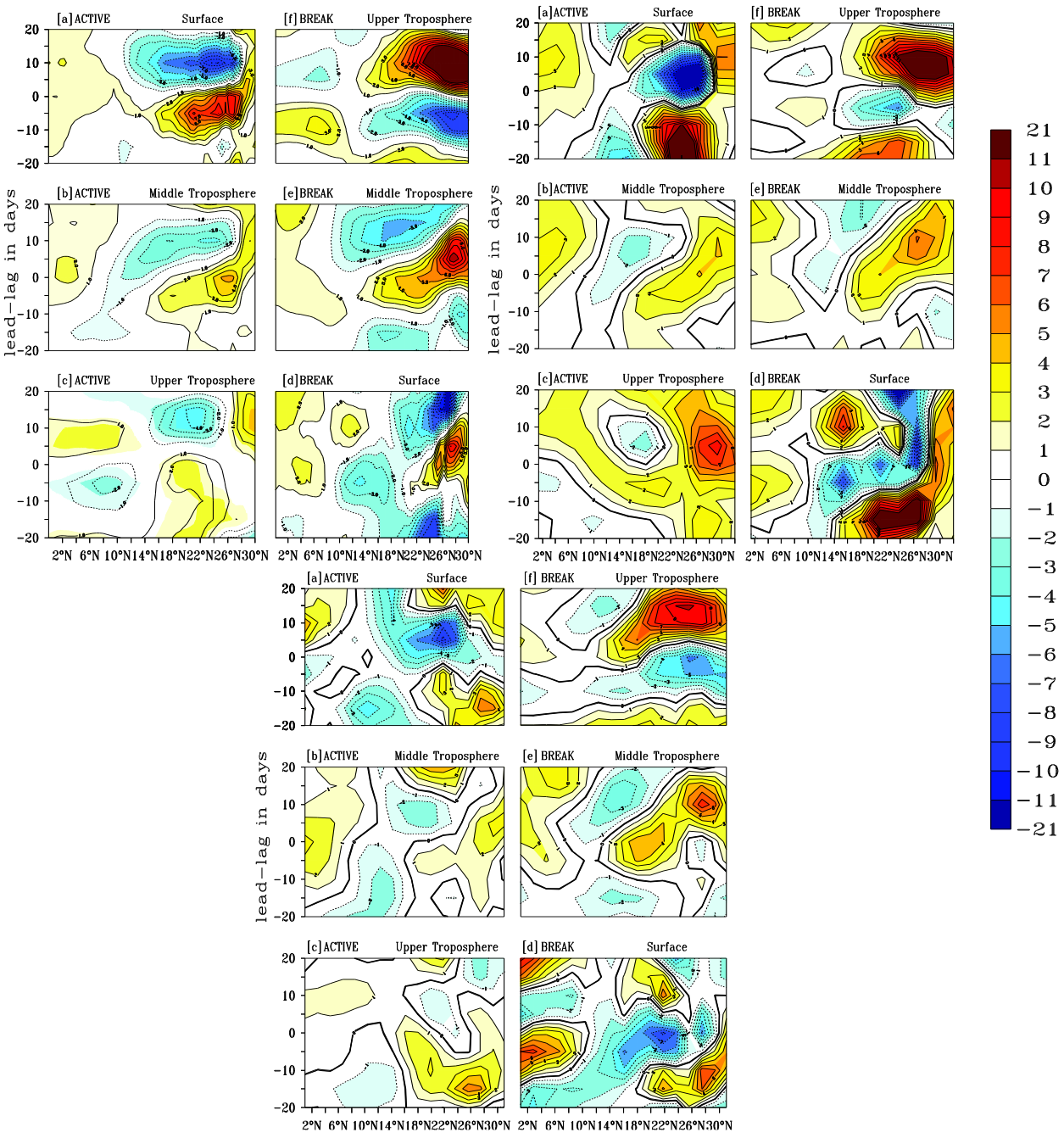

604

605 **Figure 4:** Active-break composite evolution of atmospheric CH_4 anomalies (ppb) over India, as
606 simulated by models LMDz (upper left panel), ACTM (upper right panel), and CAM-Chem
607 (lower panel). The data was averaged from 55 °E to 110 °E and is shown from the equator to 30
608 °N.

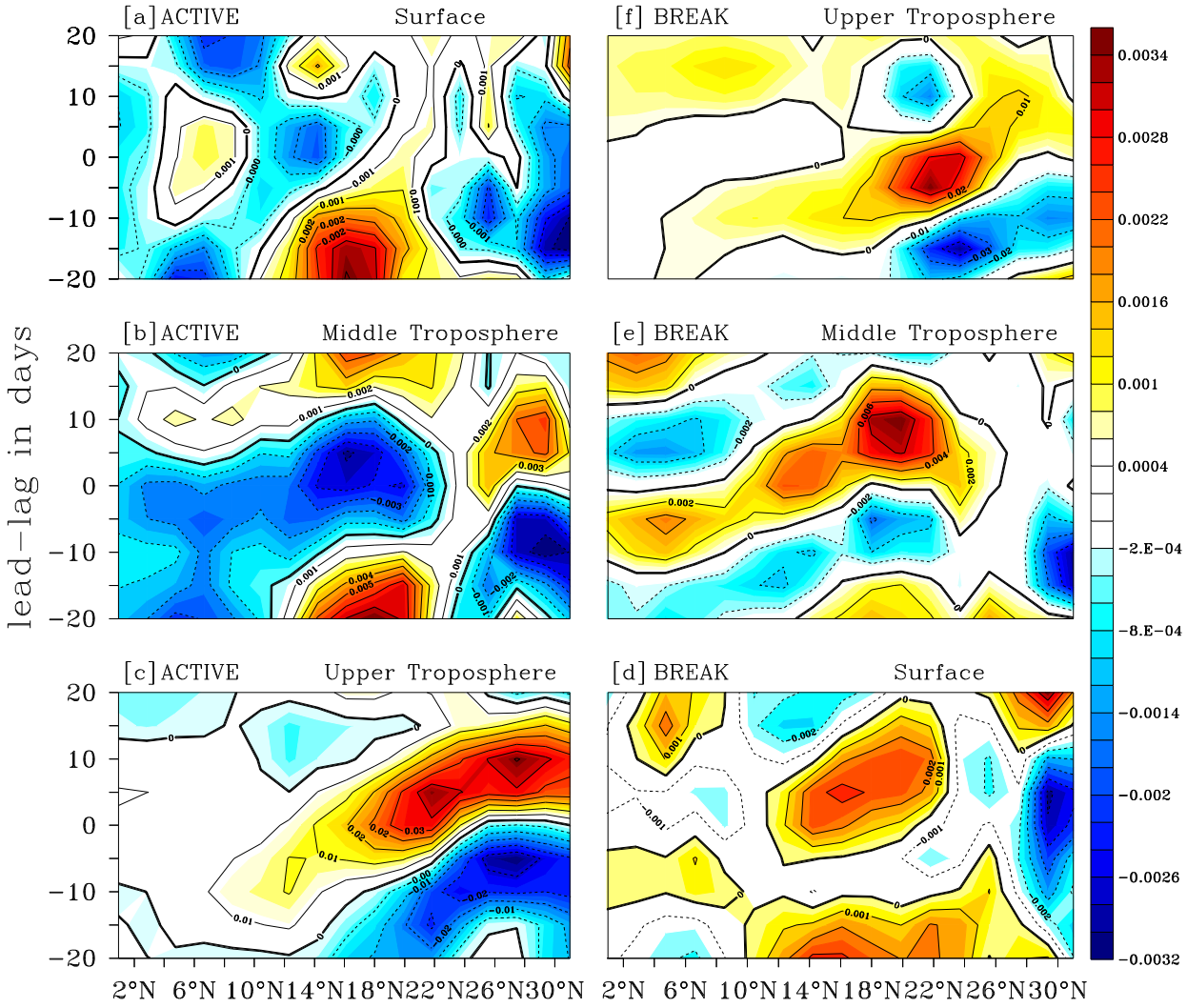

609

610 **Figure 5:** Active-break composite evolution of OH radical anomalies (ppb) over India as

611 simulated by the CAM-Chem model (averaged from 55 °E to 110 °E and shown from equator to

612 30 °N)

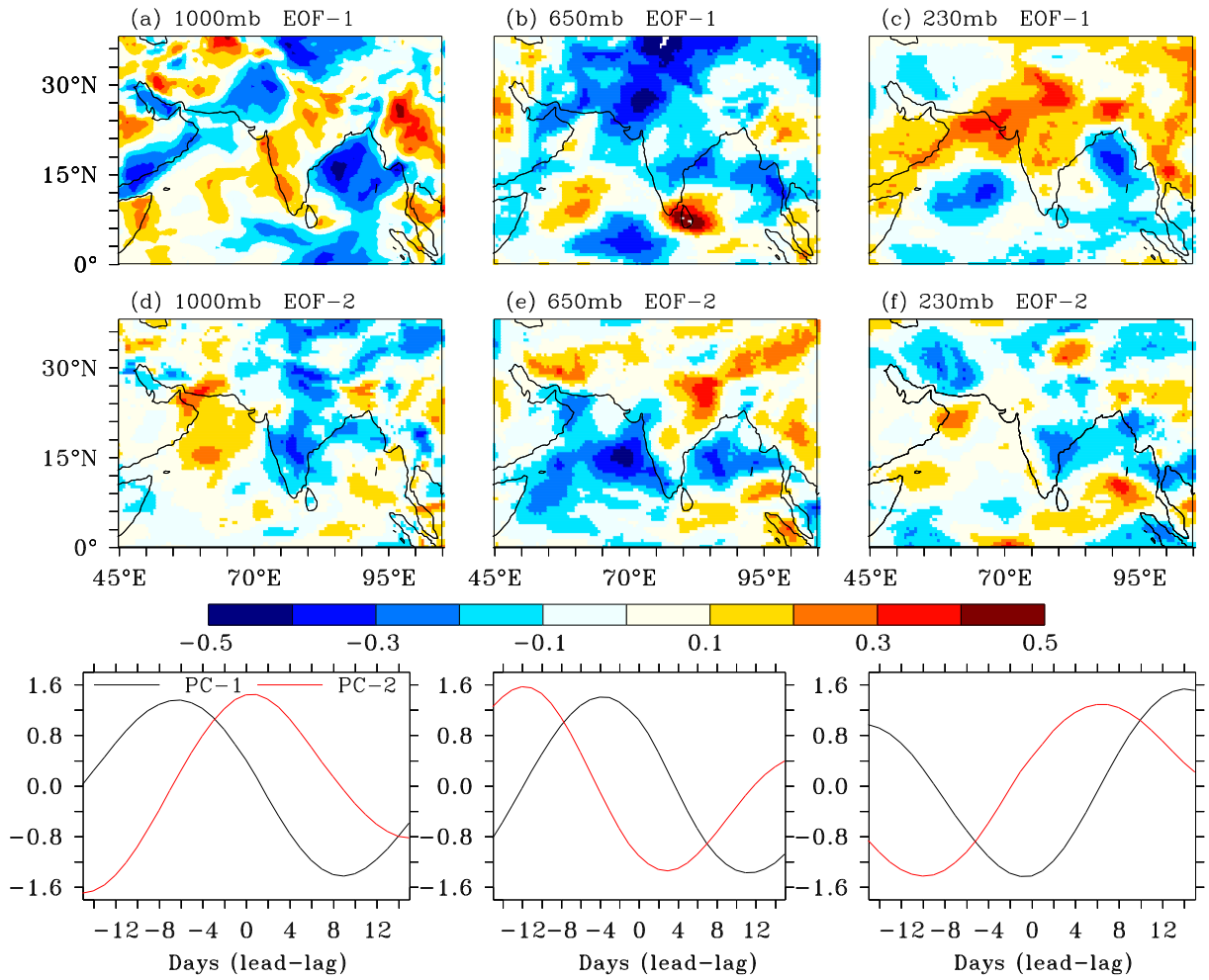

613

614 **Figure 6:** EOFs of correlation coefficients (EOF-1 and EOF-2) between OLR and CH_4
615 anomalies at: (a,d) surface (1000 mb); (b,e) middle troposphere (650 mb); and (c,f) upper
616 troposphere (230 mb). Their principle components (PC-1, PC-2) (lower Panels: left 1000mb,
617 mid 650mb, right 230 mb) in time composed of -15 to +15 days of lead-lag axis are also shown.

618